RSC Advances

ROYAL SOCIETY OF CHEMISTRY

www.rsc.org/advances

Direct preparation of PNIPAM coating gold nanoparticles by catechol redox and surface adhesion chemistry

Gema Marcelo, Marta Fernández-García

Instituto de Ciencia y Tecnología de Polímeros (ICTP-CSIC),

C/Juan de la Cierva 3, 28006-Madrid, Spain

Corresponding author: Gema Marcelo (gema.marcelo@ictp.csic.es)

Abstract

This paper describes a straightforward single-step method for the preparation and decoration of gold nanoparticles with a poly(*N*-isopropylacrylamide) (PNIPAM) shell in a water solution. This methodology is based on catechol redox and adhesion properties. PNIPAM containing a catechol ended group is used in water as both a reducing agent of $HAuCl_4$ and a capping agent of the resulting gold nanoparticles. Polyhedral gold nanoparticles are obtained at pH=11.6. However, branched gold nanoparticles are obtained at a neutral pH. This strategy for generating gold nanoparticles coated with a PNIPAM shell, especially branched gold nanoparticles, is a surfactant-free method, in particular cetyltrimethylammonium bromide, which is widely employed in the generation of branched gold nanoparticles and many toxicity concerns have been raised about its use. Nowadays, one of the topics on which gold nanoparticle research is focused, is the use of branched gold nanoparticles and their modification with a polymer shell to be employed in surface enhanced Raman scattering (SERS) detection. The branched gold nanoparticles coated with a PNIPAM shell described here present a high colloid stability in water and are used in the direct SERS detection of pyrene in water solution allowing the pyrene SERS detection at a concentration of 0.13 μM.

Introduction

Gold nanoparticles display a strong absorption band in the UV-visible-NIR light region; the physical origin of this phenomenon is the collective oscillation of the conduction-band electrons induced by the interacting electromagnetic field, the so-called localized surface plasmon resonance (LSPR). The gold nanoparticles optical response is strongly dependent on the size, shape and dielectric properties of the medium.[1] This feature makes gold nanoparticles greatly interesting to applications of different fields such as electronics,[2] photonics,[3] biomedicine (photo thermal therapy)[4] and sensing[5].

The design of gold nanoparticles coated with a specific polymeric material can combine unique optical properties of the metallic core with the properties of the polymeric layer. The adsorption of polymers onto the gold particles can affect the LSPR properties,[6] as well as the stability of colloidal suspension.[7,8] The ability to tune the organic outer layer broadens the technological application capacity of these hybrid materials. In particular, modifications to be applied in sensing[9] or surface-enhanced Raman scattering (SERS)[10,11] are examples of applications where gold nanoparticles are receiving increasing attention.

SERS is a powerful spectroscopy technique based on the strong increase of the Raman signals of molecules which have been attached to nanometer sized metallic structures.[12-14] One of the requirements for obtaining a strong SERS signal depends on the molecule to be analyzed and its affinity to metal surfaces. Molecules containing thiol, nitrile, amine and carboxylic groups provide good signals for ultrasensitive analytical purposes. Therefore molecules with no affinity, like polycyclic aromatic hydrocarbons, would not generate a strong enough SERS signal. In this sense, the functionalization of metallic surfaces with different groups in order to increase the concentration

of molecules close to the plasmonic surface and thus broaden the range of molecules to be detected by SERS is gaining consideration nowadays.[11-22] Among these strategies, the coating with a poly(*N*-isopropylacrylamide) (PNIPAM) shell has been demonstrated to be an efficient trap especially for hydrophobic analytes.[11] Recently, researchers have been focusing on the use of branched gold nanoparticles and their modification with a polymer shell in SERS detection since these metallic structures present a strong enhanced activity.[23,24] Several synthetic approaches have been reported for generating these branched gold nanoparticles.[18,24-36] Most of these methods are based on the chemical reduction of a gold salt in the presence of poly (vinylpyrrolidone) or surfactans like sodium dodecyl sulfate and cetyltrimethylammonium bromide.[25,26,29,30,33-36]

PNIPAM is the most studied and employed thermo-sensitive polymer. It undergoes a sharp coil-to-globule transition and, subsequently, a phase separation above its lower critical temperature solution (LCST).[37-39] Therefore, the conjugation of PNIPAM with gold nanoparticles provides thermo-responsive colloids. Different approaches are followed to modify gold nanoparticles with a PNIPAM coating: (i) Conjugation with Au nanoparticles of a PNIPAM bearing thiol groups;[40] (ii) employing a charged diblock copolymer containing PNIPAM and a cationic block that affords electrostatic interaction with the negative charged gold surface;[41] (iii) layer-by-layer assembly;[18] and (iv) grafting vinyl groups at the gold nanoparticle surface to induce PNIPAM polymerization.[11,18,42]

Recently, catechol containing molecules have been studied enthusiastically because of their unique reductive properties and also for their exceptional binding affinities to various substrates including metals, metallic oxides, and organic surfaces.[43,44] The key feature of redox activity is based on the hydroxyphenol groups undergoing self-conversion into their quinone forms by releasing protons and electrons under mild reductive conditions.[45,46] So, a novel strategy based on catechol redox activity to synthesize polymer-coated metal nanoparticles through reduction of gold cations with 3,4-dihydroxyphenylalanine containing polymer, either poly(ethylene glycol) or polyethylenimine has been described.[47,48]

In the present work, the catechol redox chemistry was selected to prepare and functionalize in a straightforward manner gold nanoparticles with a PNIPAM shell in water. PNIPAM containing a catechol group in its structure is synthesized by atom transfer radical polymerization (ATRP) by using an ATRP initiator prepared by dopamine modification. This polymer was characterized and used to form gold nanoparticles decorated with PNIPAM (Au@PNIPAM NPs) in water in the same step and in the absence of any surfactant or reducing agent. Thus, the present strategy can be considered an environmentally friendly process. Different experimental conditions were studied in the preparation of the gold nanoparticles. Not only the size of Au@PNIPAM NPs could be controlled, but their morphologic characteristic could also be tailored from polyhedral to branched nanoparticles. The potential of these Au@PNIPAM NPs in the SERS detection of pyrene was corroborated.

Experimental

Synthesis of the initiator 2-bromo-N-[2-(3,4-dihydroxyphenyl)ethyl] isobutyryl amide. The synthesis of the ATRP initiator based on dopamine was performed using a similar method described elsewhere.[49] Briefly, a 250 mL round-bottomed flask was charged with borax ($Na_2B_4O_7 \cdot 10H_2O$, 3.83 g, 10 mmol) and 100 mL water. The solution was degassed with argon for 30 min, and then dopamine HCl (1.9 g, 10 mmol) was added. The reaction mixture was stirred for 15 min and the pH was adjusted to 9-10 with Na_2CO_3 aqueous solution (3.99 g, 32 mmol). The resulting solution was cooled down in an ice bath, and 2-bromoisobutyryl bromide (1.6 mL, 2.34 g, 10 mmol) was added drop-wise via a syringe. After that, the reaction mixture was allowed to reach room temperature and stirred for 24 h under argon, maintaining the pH of the solution at 9-10 during the reaction. Then, the mixture was acidified to pH = 2 with a 6 M HCl aqueous solution and extracted with EtOAc (3 × 100 mL). The organic extracts were dried over $MgSO_4$, and the filtered solvent was evaporated under reduced pressure to give a brown liquid. The crude product was purified by silica gel column chromatography (4% MeOH in $CHCl_3$) to give a white solid (yield 60 %).

^{1}H-NMR (300 MHz, MeOH-*d4*), δ (ppm): 6.67 (d, 1H, Aryl-*H*), 6.64 (s, 1H Aryl-*H*), 6.53 (d, 1H, Aryl-*H*), 3.34 (q, 2H, Aryl-C*H₂*-CH₂-NH) and 2.64 (t, 2H, Aryl-CH₂-C*H₂*-NH), 1.88 (s, 6H, CO-C(C*H₃*)-Br).

Synthesis of catechol functional PNIPAM via ATRP

The synthesis of catechol-PNIPAM was carried out by ATRP using the catechol initiator and CuCl/Me₆TREN as metal activator and ligand, respectively (Scheme 1). The initiator (0.32 g, 10.4 mol), NIPAM (8.3 g, 10.4 mol), CuCl (65 mg, 10.4 mol), Me₆TREN (190 mL, 10. 4 mol) and a DMF:H₂O mixture (v:v 3:1, 8 mL) were added to a 25 mL Schlenk flask. After it was degassed with argon for 1h, the flask was kept under a slight pressure of argon. The reaction mixture was immersed in an oil bath at 25 ºC (room temperature, rt) for polymerization. The reaction was stopped after 24h by diluting with THF (20 mL), and the mixture was passed through an alumina column to remove the copper catalyst. The polymer was purified by precipitation in diethylether, collected by filtration, and dried in a vacuum for 24 h.

The number-average molecular weight and the unit numbers NIPAM were evaluated by ^{1}H-NMR comparing the integral area of the end-capped catechol proton peaks (δ= 7-6.5 ppm) and the methylene proton peak of PNIPAM (δ= 3.85 ppm), Figure S1. The molecular weight was roughly estimated to be 17500 g/mol.

Scheme 1. Schematic illustration showing a) dopa-ATRP initiator synthesis, b) *N*-isopropylacrylamide ATRP polymerization and c) Au@PNIPAMx NPs preparation.

Preparation of gold nanoparticles coated with PNIPAM (Au@PNIPAMx NPs).

Scheme 1c illustrates the formation process of gold nanoparticles coated with PNIPAM. In one series of experiments, 200 μL of either catechol-PNIPAM solution (0.22 g/mL in ultrapure deionized water) were added to 2 mL of water (pH= 11.6, adjusted with NaOH solution) while stirring. After 1 min different aliquots of HAuCl$_4$ (0.0138 M) were added. Table 1 collects the different experimental conditions. Direct observation of the gold nanoparticle formation took place

after 30 seconds by changing the solution from colorless to red. The mixtures were stirred for 30 min and after that the unattached polymer was removed by iterative centrifugation (12000 rpm) and subsequent re-suspension steps, at least four times.

To study the importance of pH in gold nanoparticle formation, 200 mL of catechol-PNIPAM (0.22 g/ml) in ultrapure deionized water were added to 2 mL of deionized water at two different pH values (7.0 and 11.6) and maintained under stirring during 1 min. After that, 50 µL of $HAuCl_4$ (0.0138 M) were added. After 120 seconds the color changed to blue when the pH of solution was adjusted at 7.0 while the color turned red at pH=11.6. The effect of the $HAuCl_4$ concentration was also studied at pH=7 (see Table 1).

Table1. Experimental conditions in the preparation of Au@PNIPAMx NPs. Mean Size values determined from TEM histograms, hydrodynamic diameters and the surface plasmon resonance (SPR) position of Au@PNIPAMx NPs.

Sample Au@PNIPAMx	V_{HAuCl4} (µL)	V_{CNIPAM} (mL)	V_{H2O} (mL)	Molar ratio $HAuCl_4$/PNIPAM	pH	TEM Size (nm)	D(DLS) (nm)	SPR λ (nm)
Au@PNIPAM1	28	0.2	2	0.15	11.6	6	10	528
Au@PNIPAM2	50	0.2	2	0.30	11.6	10	22	528
Au@PNIPAM3	100	0.2	2	0.60	11.6	18	35	534
Au@PNIPAM4	200	0.2	2	1.19	11.6	20	45	536
Au@PNIPAM5	400	0.2	2	2.38	11.6	50	$D_1=20$ $D_2=70$	560
Au@PNIPAM6	28	0.2	2	0.15	7.0	54	—	590
Au@PNIPAM7	50	0.2	2	0.30	7.0	75	—	624

Surface-Enhanced Raman Scattering (SERS). Samples for "average SERS" were prepared by adding 10 μL aliquots of pyrene in EtOH to 0.5 mL of a colloidal suspension at pH 7.0 of Au@PNIPAM7 NPs in water (6.9×10^{-4} M in gold). The final pyrene concentration ranges from 1×10^{-7} M to 1×10^{-4} M. After 30 min stirring at room temperature to allow for the thermodynamic equilibrium to be reached, the mixture was treated at 55 ºC under stirring for 5 min in order to remove the maximum amount of EtOH. The loss of water was taken into account in order to keep the initial concentration of gold nanoparticles constant. Average SERS was directly recorded from these suspensions.

Results and Discussion

The present work describes the direct preparation and functionalization of gold nanoparticles with a PNIPAM shell, Au@PNIPAMx NPs (where x refers to the preparation conditions, see Table 1). This approach is based on both the adhesion and redox activity in water of the catechol group[46,47] contained in a PNIPAM chain. This methodology presents many advantages such as: (i) the direct preparation and functionalization of gold nanoparticles with either polymer or catechol-based molecules; (ii) it takes place in water; (iii) it is a surfactant-free method unlike other methods reported in literature; (iv) it allows control over the polymer surface because the polymer is designed according to the desired application and is characterized prior to the preparation of gold nanoparticles and (v) it allows the size and morphology of gold nanoparticles to be changed. The experimental work consists of two steps. The first one involves the design of the PNIPAM chain with a catechol group at its end (catechol-PNIPAM). During the second step, the direct gold formation in water in the presence of catechol-PNIPAM, which acts as a reducer and capping agent, takes places.

Synthesis of catechol functional PNIPAM (catechol-PNIPAM).

ATRP is a tool that is extensively used in the control of the architecture and molecular weight of different polymers.[50] It was therefore selected for the preparing of a PNIPAM chain containing a catechol ended group. Dopamine is a catecholamine which has been widely studied for its adhesion properties to a wide variety of surfaces,[43,51] so several chemical modifications of its structure have been carried out. It has been modified to obtain an ATRP initiator in order to change surfaces by grafting from polymerization techniques.[49] In the present work, in accordance with what was described in literature, dopamine was chemically modified to an ATRP initiator and was used as the ATRP initiator of the NIPAM polymerization in a DMF:H_2O (3:1) medium with CuCl:MeTREN as the catalytic system.[52] The molecular weight of catechol-PNIPAM estimated by ^{1}H-NMR is ca. 17500 g/mol.

One advantage of using ATRP as a polymerization tool is that the resulting polymers contain a Br group at the chain end, which could be used for further modifications (reaction with amine groups, re-initialization of ATRP among others).[50] Therefore, the PNIPAM obtained by ATRP using the dopamine containing ATRP initiator presents a multifunctional behavior: (1) thermo responsiveness; (2) the capacity for adhesion and redox properties due to catechol groups; and (3) further modifications through chemistry of the -Br ended group.

The water solution behavior of catechol-PNIPAM at three different concentrations, 0.037 g/mL, 0.02 g/mL and 0.014 g/mL was studied by DLS. The polymer in water at 25 ºC presented hydrodynamic diameter values of 30 nm at the three analyzed concentrations. Whereas above 32 ºC, the PNIPAM chains become hydrophobic, collapse and form a macroscopic aggregated phase.

Synthesis and characterization of Au@PNIPAMx NPs.

The catechol-PNIPAM was used to prepare gold nanoparticles and functionalize their surface *in situ* in water, Au@PNIPAMx NPs (see Scheme 1). Hydroxyphenol groups undergo an oxidative self-conversion into their quinone forms by releasing protons and electrons under mild reductive conditions, which are responsible for a gold salt precursor reduction to form gold nanoparticles.[45,46]

On the other hand, the catechol group stability in water depends on the average pH value. At basic pH (pH≥8.5) in the presence of oxygen, it initially starts suffering an oxidation process and the catechol group is transformed to a quinone.[53] UV spectra of catechol-PNIPAM in water (at pH=7) showed only a band centered at 280 nm indicating no oxidation of the hydroxyphenol groups. However, a new broad band at wavelengths longer than 300 nm appeared for catechol-PNIPAM in water at pH=11.6 indicating the presence of oxidized species (spectra not shown). Consequently, the reducing agents that react with $HAuCl_4$ are different depending on the pH value. Therefore, the pH influence on the characteristics of the resulting Au@PNIPAMx NPs was analyzed. To do this, Au@PNIPAMx NPs were prepared at pH 7 and 11.6.

We will now discuss the preparations carried out at a basic pH. The direct gold nanoparticle formation and functionalization by a PNIPAM shell was achieved by simply mixing aliquots of aqueous solutions of PNIPAM (0.22 g/mL) and $HAuCl_4$ (13.8 mM) in a water solution at pH =11.6 under stirring at room temperature. Different $HAuCl_4$/PNIPAM molar ratios were studied (Table 1). Figure 1 shows the TEM images of Au@PNIPAMx NPs obtained for the different $HAuCl_4$/PNIPAM ratios at pH 11.6. Au@PNIPAMx NPs have a polyhedral morphology, which can be observed better for the higher $HAuCl_4$/PNIPAM molar ratios, Figure 1D and E. It was also observed that the size of the resulting Au@PNIPAMx NPs could be varied by changing this ratio. Histograms showing the diameter size distribution are included in Figure 2. The following conclusion could be drawn: the higher the $HAuCl_4$ concentration, the greater the Au@PNIPAM NPs size and size dispersion are. The dimension increased from a few nanometers for Au@PNIPAM1 NPs up to 80 nm for Au@PNIPAM5 NPs.
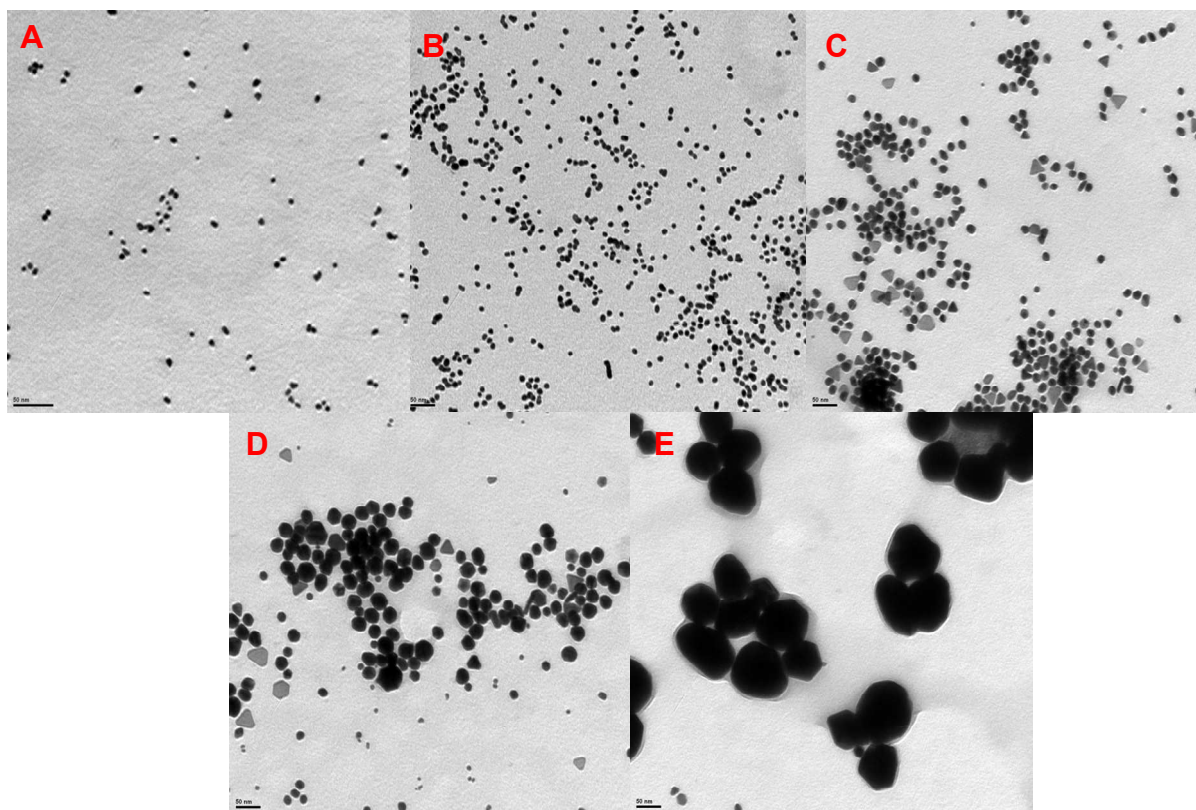
Figure 1. TEM images of Au@PNIPAM1 NP (A), Au@PNIPAM2 NPs (B), Au@PNIPAM3 NPs (C), Au@PNIPAM4 NPs (D) and Au@PNIPAM5 NPs (E). Scale bar=50 nm.
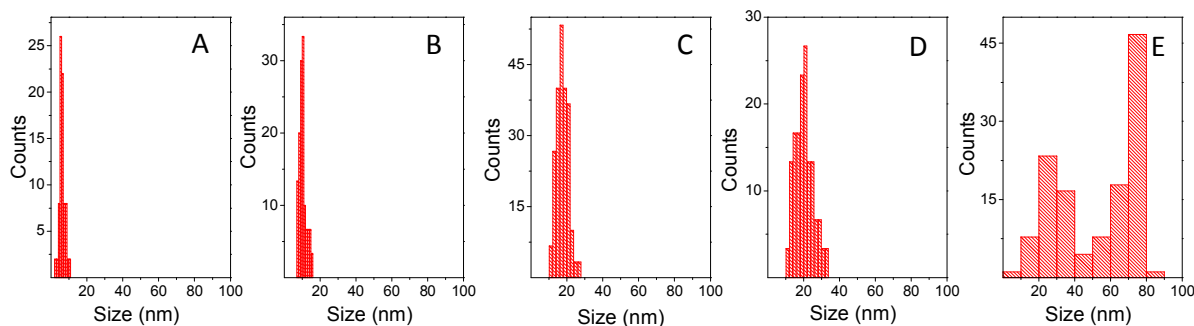
Figure 2. TEM Size Histograms of Au@PNIPAM1 NP (A), Au@PNIPAM2 NPs (B), Au@PNIPAM3 NPs (C), Au@PNIPAM4 NPs (D) and Au@PNIPAM5 NPs (E).

In order to study the pH influence on the formation of Au@PNIPAMx NPs, the preparation was carried out at pH=7 with a ratio $HAuCl_4$/PNIPAM= 0.30. The obtained nanoparticles were compared with those prepared at pH=11.6 with the same ratio, Au@PNIPAM2 NPs. Figure 3

illustrates the TEM images of gold nanoparticles synthesized at both pH values. The most notable observation was when preparation was carried out at a neutral pH, when branched gold nanoparticles were obtained. These branched nanoparticles presented larger sizes, ca. 70 nm, than those obtained at a basic pH value (ca.10 nm). This is not an exceptional case as the preparation of branched gold nanoparticles by using hydroxyphenol derivatives in water has been reported elsewhere.[46] But to the best of our knowledge, it is the first example in literature using catechol redox chemistry where gold nanoparticles are prepared *in situ* and functionalized with a PNIPAM shell and their morphologic characteristics (from polyhedral to branched nanoparticles) are changed by simply controlling the pH value of the preparation medium. A plausible reaction mechanism for the generation of these branched structures base on UV-vis kinetic studies was proposed.[46] It was considered that the formation of the branched nanoparticles occurred in two steps. Firstly, the catechol groups would release electrons to Au (III) ions generating gold nanoparticle seeds and converting themselves into quinone groups. In the second step, the quinone groups which are considered less reductive species could induce the growth of branches on the gold nanoparticle seeds during a self-polymerization process.

The increase of the $HAuCl_4$/PNIPAM molar ratio at pH=7 also increases the size of the branched

nanoparticles, like the preparation carried out at pH=11.6, Figure 4.
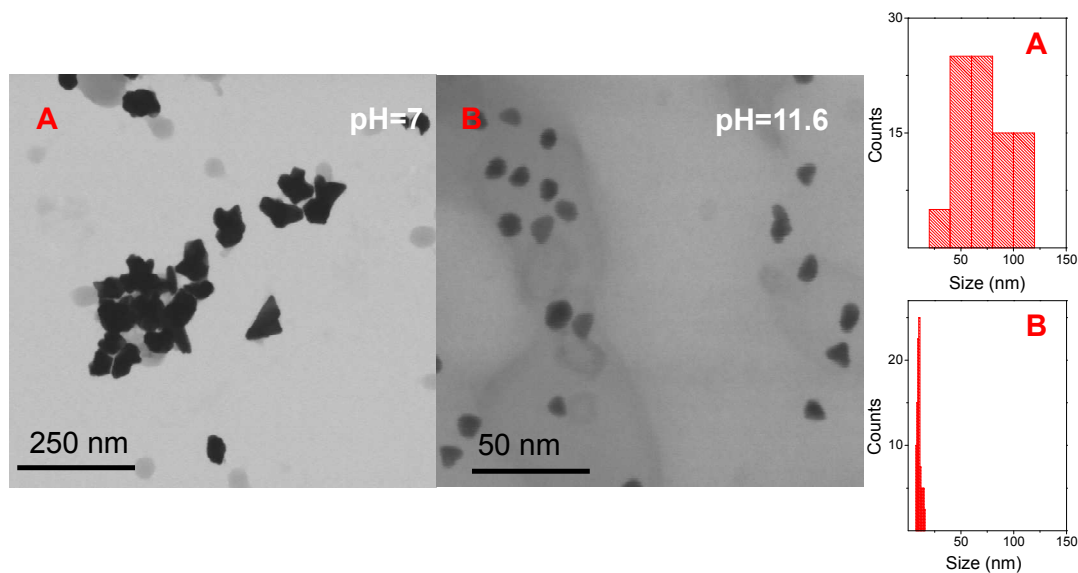
Figure 3. FE-SEM images showing the influence of the pH value of the preparation medium for a

fixed ratio $HAuCl_4$/PNIPAM= 0.30 A) pH=7, Au@PNIPAM7 NPs; B) pH=11.6, Au@PNIPAM2

NPs. TEM Size Histograms of Au@PNIPAM7 NPs (Top) and Au@PNIPAM2 NPs (Bottom).
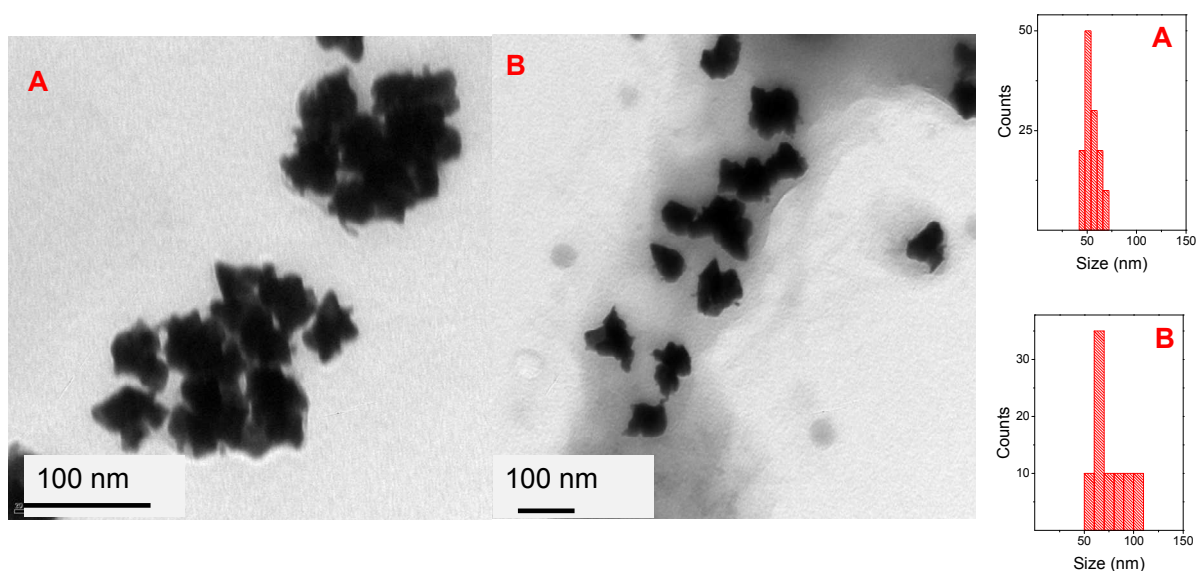
Figure 4. TEM images showing the influence of the HAuCl$_4$/PNIPAM ratio in the preparation of Au@PNIPAM NPs at pH=7. A) HAuCl$_4$/PNIPAM= 0.12, Au@PNIPAM6 NPs and B) HAuCl$_4$/PNIPAM= 0.30, Au@PNIPAM7 NPs. TEM Size Histograms of Au@PNIPAM6 NPs (Top) and Au@PNIPAM7 NPs (Bottom).

The success in the preparation of the Au@PNIPAMx NPs could be demonstrated by FT-IR. Figure 5A shows the FT-IR spectra between 1000 and 2000 nm of bulk catechol-PNIPAM and AuPNIPAM5 NPs as an example. The second amide C=O stretching (1640 cm-1), second amide N-H stretching (1539 cm-1), and deformation of two methyl groups (1386 and 1367 cm-1) attributable to PNIPAM are clearly visible in the spectra of the AuPNIPAM5 NPs. The spectral region between 2830 and 3020 cm^{-1} for both the Au@PNIPAMx NPs and the catechol-PNIPAM is shown in Figure 5B. This region contains the C-H stretching vibration regions of methylene and methyl groups. Some differences between the PNIPAM modifying gold surface and the catechol-PNIPAM are appreciable. The symmetric and asymmetric C-H stretch vibrations of methyl groups for PNIPAM on gold appeared shifted to lower frequencies. For the PNIPAM on gold surface v_{CH3a}= 2963 cm^{-1} and v_{CH3s}= 2856 cm^{-1} while for the catechol-PNIPAM v_{CH3a}= 2970 cm^{-1} and v_{CH3s}= 2876 cm^{-1}. The

asymmetric methylene vibration for PNIPAM on gold appeared at v_{CH2a}= 2920 cm^{-1} and for bulk

PNIPAM at v_{CH2a}= 2933 cm^{-1}. The shifts of PNIPAM on gold nanoparticles to lower frequencies in

relation to catechol-PNIPAM frequencies are an indication of more ordered/restricted environments

on gold nanoparticle surfaces.[54]
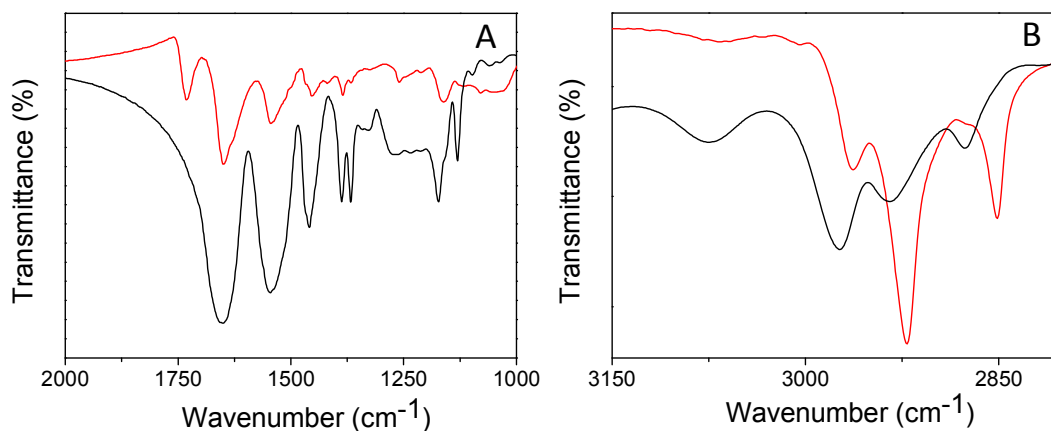
Figure 5. A: FT-IR spectra of Au@PNIPAM5 NPs (——) and catechol-PNIPAM (——). B: FTIR

spectra in the aliphatic region

The behavior of the Au@PNIPAMx NPs obtained at a basic pH in water at 25 ºC was determined

by DLS. The particles remained stable in water and aggregation was not detected during the

experiment (2 h at least). Figure 6A depicts the size distributions by number at 25 ºC for

Au@PNIPAMx NPs and the obtained average hydrodynamic diameter values are also included in

Table 1. The size distributions were shifted to higher values with the increment of a

HAuCl$_4$/PNIPAM ratio. The hydrodynamic diameters were 10, 22, 35, 45 and 70 nm for

Au@PNIPAM1 NPs, Au@PNIPAM2 NPs, Au@PNIPAM3 NPs, Au@PNIPAM4 NPs and

Au@PNIPAM5, respectively. Size distribution variations with a HAuCl$_4$/PNIPAM ratio are in

agreement with the trend showed by the TEM study. Therefore, DLS and TEM demonstrated that

the size of the Au@PNIPAMx NPs could easily be varied by simply changing the

HAuCl$_4$/PNIPAM ratio.
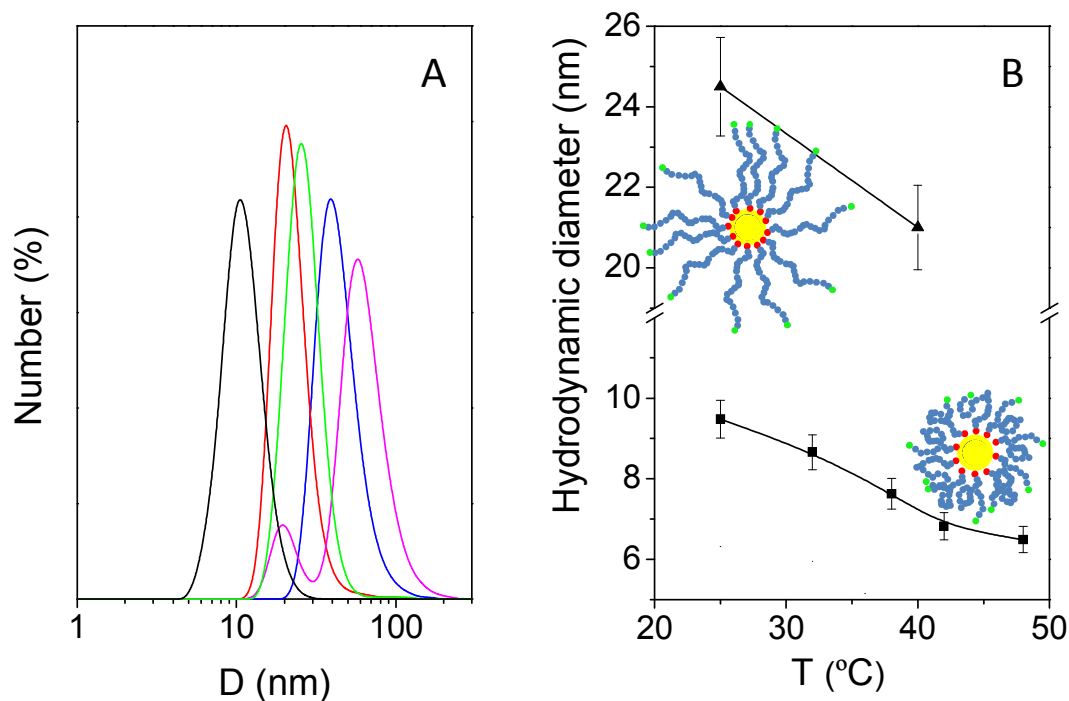
Figure 6. A) Size distributions by number for: Au@PNIPAM1 NPs (——), Au@PNIPAM2 NPs (——),

Au@PNIPAM3 NPs (——), Au@PNIPAM4 NPs (——) and Au@PNIPAM5 NPs (——). B)

Hydrodynamic diameter as a function of temperature for the samples: Au@PNIPAM1 NPs (—●—)

and Au@PNIPAM2 NPs (—▲—). Each error bar indicates the standard deviation.

As was mentioned in the introduction, the coating of gold nanoparticles with a PNIPAM shell

provides to the Au@pNIPAMx NPs of potential thermo-responsive behavior. The variation of

water colloid stability with temperature was determined by DLS. There were differences between

the aggregation behavior of bulk catechol-PNIPAM and Au@pNIPAMx NPs. Whereas catechol-

PNIPAM suffered a fast precipitation after surpassing LCST, the aggregation of nanoparticles

above PNIPAM LCST was not observed in any of the systems studied, even after increasing the

temperature up to 42 ºC and maintaining that temperature for three hours. Au@PNIPAM1 and

Au@PNIPAM2 NPs, because of their narrower size distributions, were selected to show the

influence of the thermorespose PNIPAM coating on the size of Au@PNIPAMx NPs as a function

of temperature. Figure 6B demonstrates that the increase in temperature led to a slight decrease of the hydrodynamic diameter, which could be explained in terms of a progressive collapse of the PNIPAM shell. This collapse was ca. 3 nm and 4 nm for Au@PNIPAM1 NPs and Au@PNIPAM2 NPs, respectively. This shell collapse was not followed by an aggregation process. Similar behavior in terms of the aggregation absence with an increase in temperature for gold nanoparticles modified with a PNIPAM shell was reported in literature.[55] It was explained under the consideration that the nanoparticles presented very slow kinetics of aggregation.

It is well-known that the width and position of the localized surface plasmon resonance (LSPR) band are usually strongly dependent on factors such as the size and shape of the nanoparticle, the state of aggregation, the dielectric features of the metal from which the nanoparticle is composed, and the dielectric properties of the local environment in which the nanoparticles are embedded.[1,18] Figure 7A illustrates the photograph of two nanoparticle solutions of Au@PNIPAMx synthetized at both pH= 11.6 and pH= 7. In contrast to the characteristic red color of gold nanoparticles obtained at pH=11.6, the colloidal solution of the branched gold nanoparticles is blue. The LSPR spectra for the different samples are shown in Figure 6. The series Au@PNIPAM1 to Au@PNIPAM5 NPs were characterized by the typical LSPR band (Figure 7B) and its position is also sumarized in Table 1. The optical response of branched gold nanoparticles has been established to be governed by LSPR modes confined in the tips and the core of the particles. [24] The branched nanoparticles obtained at pH=7 presented a broader LSPR band whose position was 100 nm red-shifted, (see Figure 7C) corresponding to the tip localized plasmon mode. It has been established that the position of the LSPR band for the hyperbranched nanoparticles is strongly influenced by morphologic characteristics of branched nanoparticles like size of the core, number and length of branches and the angle between branches…,[24] which could explain the LSPR position differences for the branched nanoparticles obtained at two different HAuCl$_4$/PNIPAM ratios.
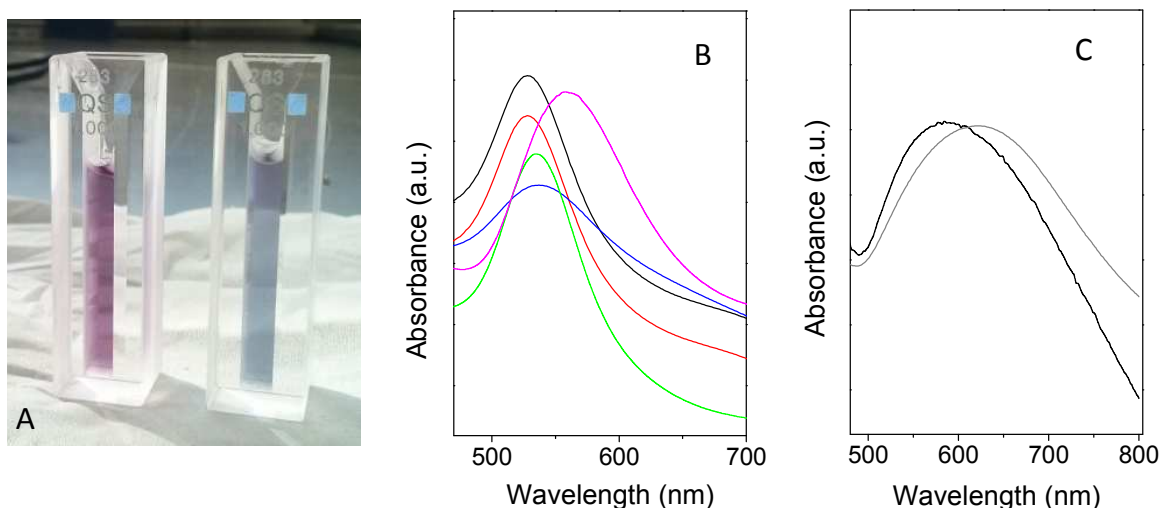
Figure 7. A) Image of colloid solution of Au@PNIPAM3 NPs (left) and Au@PNIPAM8 NPs (right) in water. B) UV-Vis spectra for Au@PNIPAM1 NPs (—), Au@PNIPAM2 NPs (—), Au@PNIPAM3 NPs (—), Au@PNIPAM4 NPs (—) and Au@PNIPAM5 NPs (—). C) UV-Vis spectra for: Au@PNIPAM6 NPs (—), Au@PNIPAM7 NPs (—).

The water colloid stability with temperature was also determined by UV-NIR spectroscopy. The LSPR band did not change with the temperature in the range from 25 to 43 ºC (data not shown), which means that the nanoparticles remained stable and the aggregation above PNIPAM LSCT was not observed in any of the studied systems. This feature is in agreement with the colloid stability as a function of temperature previously determined by DLS. Moreover, contrary to what was expected, because of the local refractive index changes derived from the temperature-shell collapse, the collapse of the PNIPAM shell with the temperature increment observed in DLS measurements did not produce any shift in the localized surface plasmon resonance frequency of the Au@PNIPAMx NPs.

SERS pyrene detection

Branched gold nanoparticles are very interesting in SERS because under excitation with a suitable laser, the core acts like a plasmonic nanoantenna, while the tips concentrate the electromagnetic

field in their apex.[56] The main problem of their use in solution is that upon undergoing nanoparticle

aggregation the electromagnetic field in the apex is deactivated.[57] Therefore, using branched gold

nanoparticles coated with a polymer shell is very interesting as the coating avoids the direct contact

among branched gold nanoparticles. In the case of the present work, the coating with a PNIPAM

shell also provides the system with the ability to trap hydrophobic analytes. We are going to focus

on the study of the SERS detection of pyrene which belongs to the polycyclic aromatic hydrocarbon

family. It does not have any functional group to interact with gold surface by itself.

Several approaches have been described in literature to detect pyrene by SERS. Briefly, pyrene has

been detected in water solutions using SERS by using both host-guest interactions of calixarenes or

cyclodextrins and aliphatic monolayers retained onto plasmonic particles. These systems presented

detection limits of ca. 1×10^{-6} M.[15,17] In the present work, the ability of the branched Au@PNIPAM

NPs to trap and detect pyrene in a water solution was demonstrated by mixing a pyrene solution

with the water colloid solution of Au@PNIPAM7 NPs for 2 hours. After that, the mixture was

directly analyzed by Raman. A near infrared laser (λ_{exc}= 785 nm) was used to illuminate the

mixture. Figure 8A exhibits spectrum of the colloid suspension containing pyrene with a

concentration of 1.4×10^{-5} M. It correlates well with the Raman spectrum of the solid compound,[58]

which is characterized by vibrational modes at 1627, 1601, 1557, 1440, and 1398 cm^{-1} due to the

ring stretching; 1241 cm^{-1} attributed to the -C=CH in plane deformation and the 601 and 413 cm^{-1} -

C=CH out of plane deformations.

Figure 8B shows the variation in the intensity of 1241 cm^{-1} –C=CH in plane deformation Raman

mode with the concentration of the pyrene in solution. The representation of the Raman signal

intensity with the concentration is shown in Figure 8C. We did not observed any Raman signal for

a pyrene concentration of 6×10^{-8} M. The following concentration of our study was 1.3×10^{-7} M

which led to a weakly detectable pyrene Raman spectrum. Therefore, the lowest detectable

concentration of pyrene in water using the present experimental system was 1.3×10^{-7} M. Direct

Raman detection of pyrene in water in the absence of branched gold nanoparticles with the same

experimental setup was not achieved for pyrene concentrations lower than 5×10^{-3} M. The SERS

detection limit should be at least one order of magnitude lower than the values described in

literature.
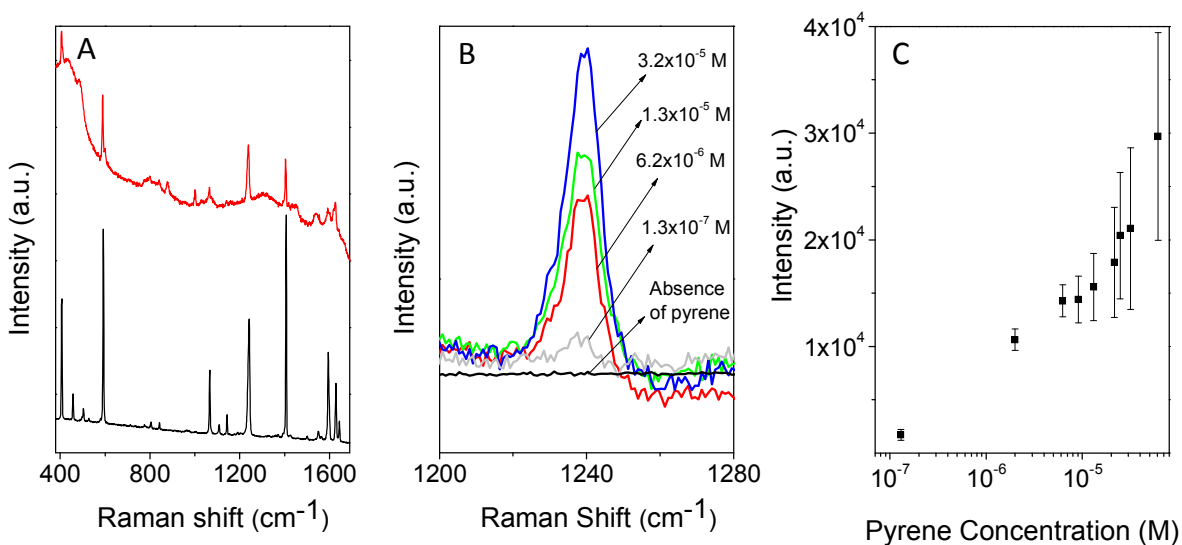
Figure 8. A) Raman spectra (λ_{exc}= 785 nm) of pyrene (—) and the water colloid suspension

containing Au@PNIPAM7 NPs and pyrene 1.4×10^{-5} M (—). B) The 1240 cm^{-1} Raman mode of

pyrene at different concentrations in the Au@PNIPAM7 NPs aqueous colloidal solution. C)

Intensity variation (at 1240 cm^{-1}) as a function of pyrene concentration.

Conclusions

The redox properties of cathecol groups in water permitted the direct formation of gold

nanoparticles and their functionalization with a PNIPAM shell in water in one step. This method

relied on the design of the PNIPAM which contained an ended cathecol group in its structure by

ATRP. In a subsequent step, the polymer in water played an essential role as the reducer of HAuCl$_4$

and coating agent in the same process. It has been demonstrated that the particle size of these

Au@PNIPAM NPs can be easily varied by modifying the HAuCl$_4$/PNIPAM ratio. It was also

determined that the morphological characteristics of gold nanoparticles could be tuned from

polyhedral to branched structures by simply changing the pH of the preparation medium. In addition, from an enviromental point of view, the advantage of this method of preparation is its forthright procedure which takes place in water in the absence of surfactants or external reducing agents. The interest of the branched gold nanoparticles coated with a PNIPAM shell in the direct SERS detection of pyrene in a water solution was also demonstrated. The lowest concentration reached for pyrene in water was 0.13 μM. Therefore, the Au@PNIPAM NPs have a potential impact on environmental investigations for identifying and quantifying organic pollutants in water by SERS.

Acknowledgements

References

1 L. M. Liz-Marzán, *Langmuir*, 2005, **22**, 32-41.

2 Y. Huang, X. Duan, Q. Wei and C. M. Lieber, *Science*, 2001, **291**, 630-633.

3 S. A. Maier, M. L. Brongersma, P. G. Kik, S. Meltzer, A. A. G. Requicha and H. A. Atwater, *Advanced Materials*, 2001, **13**, 1501-1505

4 B. Pelaz, V. Grazu, A. Ibarra, C. Magen, P. del Pino and J. M. de la Fuente, *Langmuir*, 2012, **28**, 8965-8970.

5 E. Katz and I. Willner, *Angew. Chem., Int. Ed.,* 2004, **43**, 6042-6108.

6 Y. Mai, L. Xiao and A. Eisenberg, *Macromolecules*, 2013, **46**, 3183-3189.

7 M. S. Strozyk, M. Chanana, I. Pastoriza-Santos, J. Pérez-Juste and L. M. Liz-Marzán, *Advanced Functional Materials*, 2012, **22**, 1436-1444.

8 M. Nuopponen and H. Tenhu, *Langmuir*, 2007, **23**, 5352-5357.

9 K. Saha, S. S. Agasti, C. Kim, X. Li and V. M. Rotello, *Chem. Rev.*, 2012, **112**, 2739-2779.

10 Y. Wang, B. Yan and L. Chen, *Chem. Rev.*, 2012, **113**, 1391-1428.

11 R. A. Álvarez-Puebla, R. Contreras-Cáceres, I. Pastoriza-Santos, J. Pérez-Juste and L. M. Liz-Marzán, *Angew. Chem., Int. Ed.*, 2009, **48**, 138-143.

12 M. Moskovits, *Nature*, 2010, **464**, 357-357.

13 M. Moskovits, *J. Raman Spectrosc.*, 2005, **36**, 485-496.

14 P. L. Stiles, J. A. Dieringer, N. C. Shah and R. P. Van Duyne, *Annual Review of Analytical Chemistry*, 2008, **1**, 601-626.

15 L. Guerrini, J. V. Garcia-Ramos, C. Domingo and S. Sanchez-Cortes, *Langmuir*, 2006, **22**, 10924-10926.

16 Y. Xie, X. Wang, X. Han, X. Xue, W. Ji, Z. Qi, J. Liu, B. Zhao and Y. Ozaki, *Analyst*, 2010, **135**, 1389-1394.

17 J. Du and C. Jing, *J. Phys. Chem. C*, 2011, **115**, 17829-17835.

18 C. Fernandez-Lopez, C. Perez-Balado, J. Perez-Juste, I. Pastoriza-Santos, A. R. de Lera and L. M. Liz-Marzan, *Soft Matter*, 2012, **8**, 4165-4170.

19 M. Mueller, M. Tebbe, D. V. Andreeva, M. Karg, R. A. Alvarez Puebla, N. Pazos Perez and A. Fery, *Langmuir*, 2012, **28**, 9168-9173.

20 Q. Zeng, R. Marthi, A. McNally, C. Dickinson, T. E. Keyes and R. J. Forster, *Langmuir*, 2009, **26**, 1325-1333.

21 B.-H. Jun, M. S. Noh, J. Kim, G. Kim, H. Kang, M.-S. Kim, Y.-T. Seo, J. Baek, J.-H. Kim, J. Park, S. Kim, Y.-K. Kim, T. Hyeon, M.-H. Cho, D. H. Jeong and Y.-S. Lee, *Small*, 2010, **6**, 119-125.

22 L. Guerrini, J. V. Garcia-Ramos, C. n. Domingo and S. Sanchez-Cortes, *J. Phys. Chem. C*, 2008, **112**, 7527-7530.

23 N. Pazos-Pérez, S. Barbosa, L. Rodríguez-Lorenzo, P. Aldeanueva-Potel, J. Pérez-Juste, I. Pastoriza-Santos, R. A. Alvarez-Puebla and L. M. Liz-Marzán, *J. Phys. Chem. Lett.*, 2009, **1**, 24-27.

24 S. Barbosa, A. Agrawal, L. Rodríguez-Lorenzo, I. Pastoriza-Santos, R. n. A. Alvarez-Puebla, A. Kornowski, H. Weller and L. M. Liz-Marzán, *Langmuir*, 2010, **26**, 14943-14950.

25 N. Ortiz and S. E. Skrabalak, *Crystal Growth & Design*, 2011, **11**, 3545-3550.

26 S. Chen, Z. L. Wang, J. Ballato, S. H. Foulger and D. L. Carroll, *J. Am. Chem. Soc.*, 2003, **125**, 16186-16187.

27 Xie, J. Y. Lee and D. I. C. Wang, *Chem. Mater.*, 2007, **19**, 2823-2830.

28 B. R. Danger, D. Fan, J. P. Vivek and I. J. Burgess, *ACS Nano*, 2012, **6**, 11018-11026.

29 J. Li, J. Han, T. Xu, C. Guo, X. Bu, H. Zhang, L. Wang, H. Sun and B. Yang, *Langmuir*, 2013, **29**, 7102-7110.

30 K. Pandian Senthil, P.-S. Isabel, R.-G. Benito, F. J. G. d. Abajo and M. L.-M. Luis, *Nanotechnology*, 2008, **19**, 015606.

31 J. Xie, Q. Zhang, J. Y. Lee and D. I. C. Wang, *ACS Nano*, 2008, **2**, 2473-2480.

32 E. Hao, R. C. Bailey, G. C. Schatz, J. T. Hupp and S. Li, *Nano Lett.*, 2004, **4**, 327-330.

33 Q. Wei, H.-M. Song, A. P. Leonov, J. A. Hale, D. Oh, Q. K. Ong, K. Ritchie and A. Wei, *J. Am. Chem. Soc.*, 2009, **131**, 9728-9734.

34 S. Chen, Z. L. Wang, J. Ballato, S. H. Foulger and D. L. Carroll, *J. Am. Chem.Soc.*, 2003, **125**, 16186-16187.

35 X. Kou, Z. Sun, Z. Yang, H. Chen and J. Wang, *Langmuir*, 2008, **25**, 1692-1698.

36 C. G. Khoury and T. Vo-Dinh, *J. Phys. Chem. C*, 2008, **112**, 18849-18859.

37 M. Shibayama, M. Morimoto and S. Nomura, *Macromolecules*, 1994, **27**, 5060-5066.

38 F. M. Winnik, *Macromolecules*, 1990, **23**, 233-242.

39. Fujishige, K. Kubota and I. Ando, *J. Phys. Chem*, 1989, **93**, 3311-3313.

40 M.-Q. Zhu, L.-Q. Wang, G. J. Exarhos and A. D. Q. Li, *J. Am. Chem. Soc.*, 2004, **126**, 2656-2657.

41 R. N. Pamies, K. Zhu, S. Volden, A.-L. Kjøniksen, G. r. Karlsson, W. R. Glomm and B. Nystro☐m, *J. Phys. Chem. C*, 2010, **114**, 21960-21968.

42 A. Sánchez-Iglesias, M. Grzelczak, B. Rodríguez-González, P. Guardia-Girós, I. Pastoriza-Santos, J. Pérez-Juste, M. Prato and L. M. Liz-Marzán, *ACS Nano*, 2009, **3**, 3184-3190.

43 G. Marcelo, A. Munoz-Bonilla, J. Rodriguez-Hernandez and M. Fernandez-Garcia, *Polymer Chemistry*, 2013, **4**, 558-567.

44 L. Zhang, J. Wu, Y. Wang, Y. Long, N. Zhao and Jian Xu, *J. Am. Chem.Soc* 2012, **134**, 9879−9881.

45 W.-G. Qu, S.-M. Wang, Z.-J. Hu, T.-Y. Cheang, Z.-H. Xing, X.-J. Zhang and A.-W. Xu, *J. Phys. Chem. C*, 2010, **114**, 13010-13016.

46 Y. Lee and T. G. Park, *Langmuir*, 2011, **27**, 2965-2971.

47 K. C. L. Black, Z. Liu and P. B. Messersmith, *Chem. Mater.*, 2011, **23**, 1130-1135.

48 Y. Lee, S. H. Lee, J. S. Kim, A. Maruyama, X. Chen and T. G. Park, *Journal of Controlled Release*, 2011, **155**, 3-10.

49 X. Fan, L. Lin, J. L. Dalsin and P. B. Messersmith, *Journal of the American Chemical Society*, 2005, **127**, 15843-15847.

50 K. Matyjaszewski, *Macromolecules*, 2012, **45**, 4015-4039.

51 H. Lee, S. M. Dellatore, W. M. Miller and P. B. Messersmith, *Science*, 2007, **318**, 426-430.

52 N. Pothayee, S. Balasubramaniam, R. M. Davis, J. S. Riffle, M. R. J. Carroll, R. C. Woodward and T. G. St. Pierre, *Polymer*, 2011, **52**, 1356-1366.

53 N. F. Della Vecchia, R. Avolio, M. Alfè, M. E. Errico, A. Napolitano and M. d'Ischia, *Advanced Functional Materials*, 2013, **23**, 1331-1340.

54 R. G. Snyder, H. L. Strauss and C. A. Elliger, *J. Phys. Chem.*, 1982, **86**, 5145-5150.

55 S. Chakraborty, S. W. Bishnoi and V. c. H. Pérez-Luna, *J. Phys. Chem. C*, 2010, **114**, 5947-5955.

56 F. Hao, C. L. Nehl, J. H. Hafner and P. Nordlander, *Nano Letters*, 2007, **7**, 729-732.

57 L. Rodríguez-Lorenzo, R. n. A. Álvarez-Puebla, F. J. G. a. de Abajo and L. M. Liz-Marzán, *J. Phys. Chem C*, 2009, **114**, 7336-7340.

58 P. Leyton, I. Córdova, P. A. Lizama-Vergara, J. S. Gómez-Jeria, A. E. Aliaga, M. M. Campos-Vallette, E. Clavijo, J. V. García-Ramos and S. Sanchez-Cortes, *Vib. Spectrosc.*, 2008, **46**, 77-81.
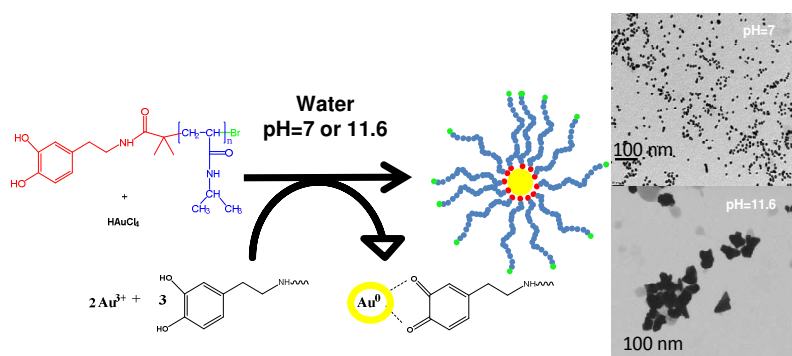
The water-stable branched gold nanoparticles coated with a PNIPAM shell allow pyrene SERS detection at a concentration of 0.13 μM